Interactions between βD372 and γ Subunit N-Terminus Residues γK9 and γS12 Are Important to Catalytic Activity Catalyzed by *Escherichia coli* F_1F_o-ATP Synthase†

David S. Lowry and Wayne D. Frasch*

Center for the Study of Early Events in Photosynthesis, School of Life Sciences, Arizona State University, P.O. Box 874501, Tempe, Arizona 85287-4501

Received December 23, 2004; Revised Manuscript Received March 28, 2005

ABSTRACT: Substitution of *Escherichia coli* F_1F_o ATP synthase residues βD372 or γS12 with groups that are unable to form a hydrogen bond at this location decreased ATP synthase-dependent cell growth by 2 orders of magnitude, eliminated the ability of F_1F_o to catalyze ATPase-dependent proton pumping in inverted *E. coli* membranes, caused a 15−20% decrease in the coupling efficiency of the membranes as measured by the extent of succinate-dependent acridine orange fluorescence quenching, but increased soluble F_1-ATPase activity by about 10%. Substitution of γK9 to eliminate the ability to form a salt bridge with βD372 decreased soluble F_1-ATPase activity and ATPase-driven proton pumping by 2-fold but had no effect on the proton gradient induced by addition of succinate. Mutations to eliminate the potential to form intersubunit hydrogen bonds and salt bridges between other less highly conserved residues on the γ subunit N-terminus and the β subunits had little effect on ATPase or ATP synthase activities. These results suggest that the βD372−γK9 salt bridge contributes significantly to the rate-limiting step in ATP hydrolysis of soluble F_1 while the βD372−γS12 hydrogen bond may serve as a component of an escapement mechanism for ATP synthesis in which $\alpha\beta\gamma$ intersubunit interactions provide a means to make substrate binding a prerequisite of proton gradient-driven γ subunit rotation.

The F_1F_o ATP synthase couples the energy provided by a transmembrane proton gradient to the production of ATP from ADP and phosphate. The intrinsic membrane complex of ab_2c_{10-14} subunits known as F_o functions as a proton channel, and the F_1[1] peripheral membrane complex of $\alpha_3\beta_3\gamma\delta\epsilon$ subunits contains one site for ATP synthesis/hydrolysis per $\alpha\beta$ heterodimer. When F_1 is purified from F_o and the membrane, it retains the ability to hydrolyze ATP (*1*).

The catalytic cycles of the three catalytic sites are staggered and coupled such that the binding of substrate to one site induces product release at an adjacent site (*2*). The three $\alpha\beta$ heterodimers form a ring around the γ subunit that rotates in response to ATP hydrolysis activity (*3*). Binding of Mg^{2+}-ATP to the empty catalytic site was found to initiate a 90° rotation of the γ subunit in F_1 from the thermophilic bacteria PS3 (*4*). After a 2 ms pause thought to involve product release, a 30° rotation of the γ subunit completes the cycle for a total of 120°. The kinetics of the 2 ms pause are consistent with the presence of sequential 1 ms steps that suggests the existence of a rate-limiting intermediate state that follows the transition state. Recent experiments suggest that the pause may occur between 80° and 40° rotation events and that the completion of a catalytic cycle at any one site involves the rotation of the γ subunit by 240° (*5*).

One catalytic site in the initial crystal structure of F_1 from bovine mitochondria (MF_1) is empty (β_E) while the other two catalytic sites contain bound ADP (β_{DP}) and the ATP analogue AMPPNP (β_{TP}), respectively (*6*). This (ADP)(AMPPNP)F_1 structure has been derived under a wide variety of conditions, which suggests that it is a low free energy conformation that may represent the ground state. A structure known as $(ADP{\cdot}AlF_4^-)_2F_1$ from bovine mitochondria contains the transition state analogue ADP-fluoroaluminate bound at two catalytic sites and has bound ADP and SO_4^{2-} at the third site (*7*). The long O−Al−O bond lengths and the presence of bound AlF_4^- rather than AlF_3 suggest that $(ADP{\cdot}AlF_4^-)_2F_1$ may represent a posttransition state intermediate conformation. In the $(ADP{\cdot}AlF_4^-)_2F_1$ structure (*7*), the portion of the γ subunit used to attach a probe to observe rotation is rotated approximately 20° relative to the (ADP)(AMPPNP)F_1 structure (*6*). However, the γ subunit C-terminus in both structures is nearly in the same position such that the helical coiled coil of the γ subunit is more tightly wound in the $(ADP{\cdot}AlF_4^-)_2F_1$ structure.

The differences in the winding of the coiled coil between the structures are evident in the interactions between the γ subunit N-terminus and the β subunits. In (ADP)(AMPPNP)-F_1, β_{DP}D386 forms a salt bridge with γR8 (Figure 1A). If

† This work was supported by NIH Grant GM-50202 to W.D.F.

* To whom correspondence should be addressed. E-mail: frasch@asu.edu. Tel: (480) 965-8663. Fax: (480) 965-6899.

[1] Abbreviations: AMPPNP, adenylyl imidodiphosphate; F_1, the extrinsic membrane associated portion of the F_1F_o ATP synthase; EF_1, the F_1 from *Escherichia coli*; MF_1, the F_1 from bovine mitochondria; (ADP)(AMPPNP)F_1, the F_1 structure that contains ADP and AMPPNP at the first and second catalytic sites; $(ADP{\cdot}AlF_4^-)_2F_1$, the F_1 structure that contains $ADP{\cdot}AlF_4^-$ at two catalytic sites and ADP and SO_4^{2-} at the third site.

10.1021/bi047293j CCC: $30.25
Published on Web 04/23/2005

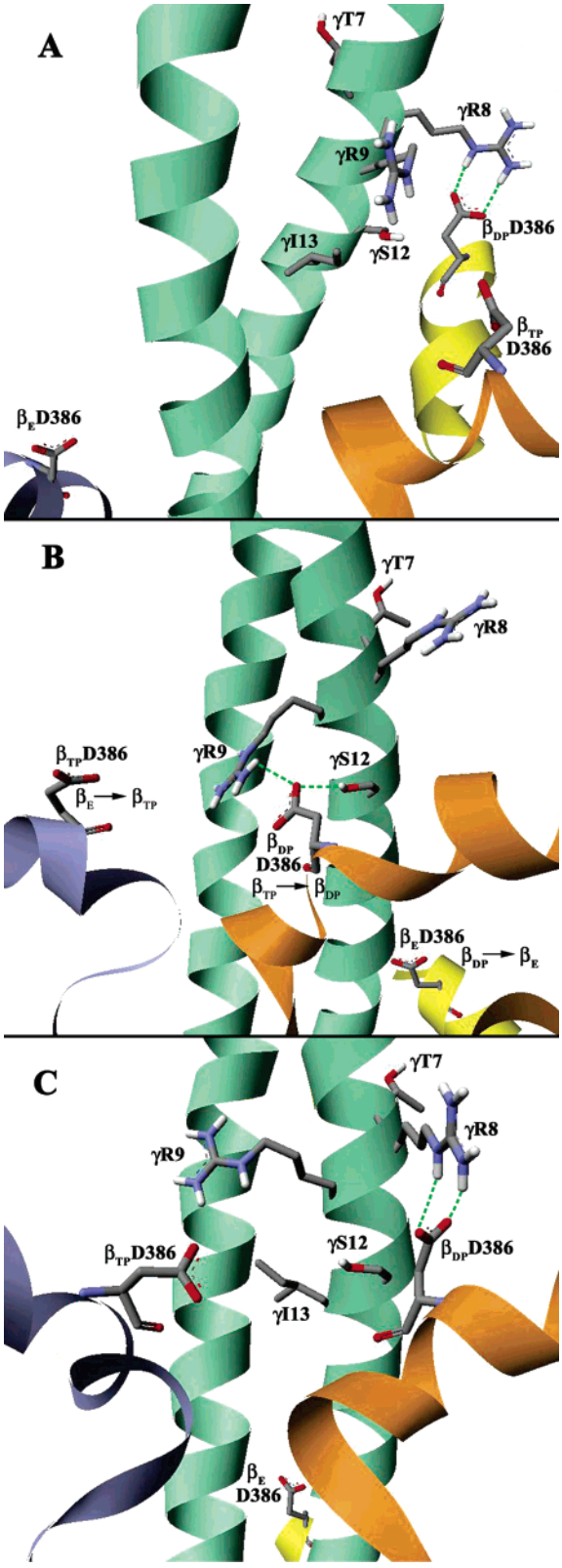

FIGURE 1: Interactions between β subunits and the γ subunit N-terminus of F_1 from bovine mitochondria. (A) (ADP)(AMPPNP)-F_1 (*6*) interactions between βD386 ($EF_1\beta$D372) and the γ subunit N-terminus (green). (B) $(ADP{\cdot}AlF_4^-)_2F_1$ (*7*) interactions between βD386 and the γ subunit N-terminus from the perspective that the γ subunit has rotated about 100° relative to (A) such that the conformational changes $\beta_{TP} \rightarrow \beta_{DP}$, $\beta_{DP} \rightarrow \beta_E$, and $\beta_E \rightarrow \beta_{TP}$ have occurred. (C) (ADP)(AMPPNP)F_1 interactions from the perspective that the γ subunit has rotated about 20° relative to (B). Images are reproduced from Protein Data Bank files 1E1Q (A, C) and 1H8E (B) using Web Lab Viewer from Molecular Simulations, Inc.

the $(ADP{\cdot}AlF_4^-)_2F_1$ structure represents the intermediate state during catalysis, then a 100° rotation of the γ subunit results in the conversion of β_{TP} to β_{DP}, and the β_{DP}D386 forms a salt bridge with γR9 and a hydrogen bond with γS12 (Figure 1B). Upon relaxation of the coiled coil to the ground state structure, the γ subunit N-terminus is rotated such that β_{DP}D386 forms a salt bridge with γR8 (Figure 1C).

Salt bridges between MF_1 residues γR254 and β_ED316 and β_ED319 in the catch loop and hydrogen bonds between γQ255 and catch loop residues β_ED316 and β_ET318 were recently found to be very important for both ATP synthesis and hydrolysis activity in F_1 from *Escherichia coli* (EF_1) (*8*). Site-directed mutants of EF_1 that eliminated the shortest and/or multiple hydrogen bonds at this location had the greatest effects on catalytic activity. During ATP synthesis, these and other hydrogen bonds and salt bridges between the γ subunit and the $(\alpha\beta)_3$ ring have been proposed to prevent proton gradient-driven rotation of the γ subunit until the empty catalytic site binds substrate (*8*, *9*). Tight coupling between the proton gradient and ATP synthesis would be maintained if these intersubunit bonds were broken only by the binding of substrate. The intersubunit hydrogen bonds and salt bridges that contribute to this escapement mechanism are likely to extend beyond the catch loop. We now report the effects of EF_1 mutations that eliminate the salt bridges and hydrogen bonds between the γ subunit N-terminus and $EF_1\beta$D372 ($MF_1\beta$D386). The results indicate that the γS12 and β_{DP}D386 hydrogen bond and the γR9 and β_{DP}D386 salt bridge that appear in the $(ADP{\cdot}AlF_4^-)_2F_1$ structure are important for ATP synthesis and hydrolysis, respectively.

EXPERIMENTAL PROCEDURES

Strains and Plasmids. The parent plasmid and *E. coli* strain used in this study are the same as described previously (*8*). All site-directed mutagenesis for the current study was performed in plasmid pXL1 using the QuikChange XL site-directed mutagenesis kit (Stratagene). The oligonucleotide primers for the creation of each mutant are shown in Table 1. The F_1-ATPase in the XL10 strain of *E. coli* contains a 6×His tag on the α subunit and γS193C mutation as described (*8*). Methods for culture growth and purification of EF_1 were carried out as described by Greene and Frasch (*8*). Growth yields in limiting glucose were measured using a modification of the procedure of Senior et al. (*10*). Strains were grown in 1 L volumes of minimal medium containing 3 mM glucose. Optical density measurements at 600 nm were taken at 1 h intervals until stationary phase was reached.

ATPase Rate Determination. ATPase activity was determined using an ATP-regenerating coupled-assay mixture at pH 8.0 containing 50 mM Tris-HCl, 10 mM KCl, 2 mM Mg^{2+}-ATP, 2.5 mM phosphoenolpyruvate, 50 μg/mL pyruvate kinase, 50 μg/mL lactic dehydrogenase, 200 μg/mL NADH, and 3 nM EF_1. The assay was monitored by absorbance change at 340 nm. Analyses were done with either a Cary 50 or Cary 100 Bio UV−vis spectrophotometer (Varian) equipped with a stir-control Peltier device. The reactions were initiated by addition of EF_1 to the mixture. ATPase rates were calculated from data collected 6−8 min after addition of EF_1 in order to minimize inhibition caused by entrapped Mg^{2+}-ADP (*11*). Calculations of the enthalpic and entropic components of the free energy of activation from

Table 1: Primers Used To Generate Mutant Strains[a]

mutant strain	mutagenic primer
β-D372V	5′-TATCAGGAACTGAAA*GTC*ATCATCGCCATCCTG-3′
γ-R7I	5′-GGCGCAAAAGAGATA*ATT*AGTAAGATCGCAAGC-3′
γ-S8A	5′-GCAAAAGAGATACGT*GCT*AAGATCGCAAGCGTC-3′
γ-K9I	5′-AAAGAGATACGTAGT*ATT*ATCGCAAGCGTCCAG-3′
γ-S12A	5′-CGTAGTAAGATCGCA*GCC*GTCCAGAACACGCAA-3′
γ-K9I/S12A	5′-CGTAGT*ATT*ATCGCA*GCC*GTCCAGAACACGCAA-3′

[a] Codons containing changes are italicized and underlined. Complementary antisense primers (not shown) were also used in each mutagenesis reaction.

Arrhenius plots were determined as described by Greene and Frasch (*8*).

Fluorometric Assays. Measurement of electrochemical gradients was carried out using a modification of the procedure described by Shin et al. (*12*) in which 10 mg of membrane vesicles was suspended in a 2 mL volume containing 50 mM Tris-HCl, 2 mM $MgCl_2$, 140 mM KCl, 1 μg/mL valinomycin, and 1 μM acridine orange, pH 8.0. To initiate the quenching reactions, succinate or ATP was added to a final concentration of 2 mM. To dissipate established gradients, carbonyl cyanide *m*-chlorophenylhydrazone (CCCP) was added to a final concentration of 1 μM. Fluorescence at 530 nm (excitation at 490 nm) was monitored on a SPEX Fluoromax fluorometer.

RESULTS

Isolation and Recovery of F_1 from Wild-Type and Mutant Strains. The F_1-ATPase was purified from cells grown to late log phase on minimal medium containing 30 mM glucose. The yield of F_1-ATPase purified from the site-directed mutants was approximately the same as that isolated from the XL10 (wild-type) strain. In each case the purified F_1 contained all five subunits as determined by SDS−polyacrylamide gel electrophoresis (data not shown). These results suggest that these mutations did not significantly affect the synthesis and assembly of the enzyme.

Growth Characteristics with Succinate and Limiting Glucose on Minimal Medium. The relative ability of the mutant and wild-type strains to grow via oxidative phosphorylation on minimal medium in the presence of succinate is summarized in Table 2. As a negative control that the growth rate of *E. coli* on minimal medium with succinate was dependent on the rate of ATP synthesis catalyzed by the F_1F_o ATP synthase, growth curves were also determined on the same medium using *E. coli* strain AN887 (*13*) that does not express the enzyme due to a suppression of the endogenous *unc* operon. The rates of log phase growth of the γK9I/S12A double mutant and βD372V were 1% and 3% of XL10, respectively. The $(ADP{\cdot}AlF_4^-)_2F_1$ structure from bovine mitochondria shows that these residues form a salt bridge and hydrogen bond between the γ and β_{DP} subunits (*7*). Although the γS12A mutation had similar growth on succinate to these mutant strains, the γK9I mutation did not affect the rate of succinate-dependent growth significantly. Consequently, the inability of the *E. coli* strain that contains the γK9I/S12A double mutant to grow on succinate primarily reflects the consequences of γS12A. On the basis of these results, only the hydrogen bond observed between the residues equivalent to $EF_1\beta$D372 and γS12 in the $(ADP{\cdot}AlF_4^-)_2F_1$ structure from bovine mitochondria is important for *E. coli* F_1F_o ATP synthase activity. The sequence comparisons of F_1 from bovine mitochondria, *E. coli*, and the thermophilic bacterium PS3 in this region of the γ subunit are shown in Table 3. It is noteworthy that although γS12 is highly conserved (*14*), and the γS12A mutation decreased succinate-dependent growth in *E. coli* by 2 orders of magnitude, alanine is the naturally occurring residue at this position in F_1 from PS3.

Table 2: Comparison of Relative Ability of XL10 and Mutant Strains To Grow Utilizing Succinate or Limiting Glucose as Sole Carbon Source and of Purified F_1-ATPase To Hydrolyze ATP[a]

	growth rate,[b] 30 mM succinate		growth yield,[c] 3 mM glucose			
strain	ΔOD/h	% XL10	max OD	% XL10	k_{cat} at 25 °C[d]	% XL10 k_{cat}
XL10	0.1044	100	0.658	100	115	100
γR7I	0.0995	95	0.643	98	112	97
γS8A	0.1079	103	0.634	96	115	100
γK9I	0.0918	88	0.597	91	58	50
γS12A	0.0015	1	0.434	66	126	110
γK9I/S12A	0.0010	1	0.366	56	68	59
βD372V	0.0031	3	0.465	71	133	116
AN887	0	0	0.422	64	ND[e]	ND

[a] All measurements are mean values taken from a minimum of three replications for each strain. [b] Cell density was measured as the optical density at 600 nm, and the rate of growth was determined as the slope at log phase. [c] Measured as the maximum optical density at 600 nm achieved upon reaching stationary phase. [d] Conditions for Mg^{2+}-ATPase activity of soluble F_1 were as described in Experimental Procedures. [e] Not determined.

Table 3: Sequence Comparisons of F_1-ATPase γ Subunit from Bovine Mitochondria, *E. coli*, and the Thermophilic *Bacillus* sp. PS3[a]

	residue						
strain	7	8	9	10	11	12	13
bovine mitochondria	T	R	R	L	K	S	I
E. coli	R	S	K	I	A	S	V
thermophilic PS3	K	T	R	I	N	A	T

[a] Sequences taken from Hong and Petersen (*14*).

In the (ADP)(AMPPNP)F_1 structure, βD386 ($EF_1\beta$D372) forms a salt bridge with γR8 (*6*). Although this latter residue is not conserved in *E. coli*, $EF_1\gamma$S8 is still capable of forming a hydrogen bond with $EF_1\beta$D372. However, the succinate-dependent growth of the *E. coli* strain that contains the γS8A mutation is not significantly different from that of XL10, indicating that this putative hydrogen bond is not necessary for ATP synthase activity. It appears that the arginine and hydroxyl group at positions 7 and 8 of *E. coli* have been inverted in bovine mitochondria (Table 3), raising the possibility that the salt bridge in the ground state may contain $EF_1\gamma$R7 in lieu of $MF_1\gamma$R8. The succinate-dependent growth

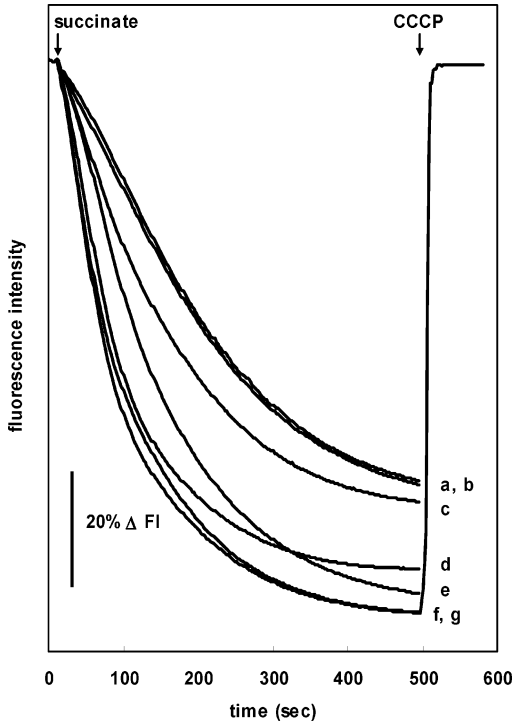

FIGURE 2: Formation of succinate-dependent electrochemical gradients measured by fluorescence quenching of 1 μM acridine orange in membrane vesicles from strains βD372V (a), γK9I/S12A (b), γS12A (c), γS8A (d), γR7I (e), γK9I (f), and XL10 (g).

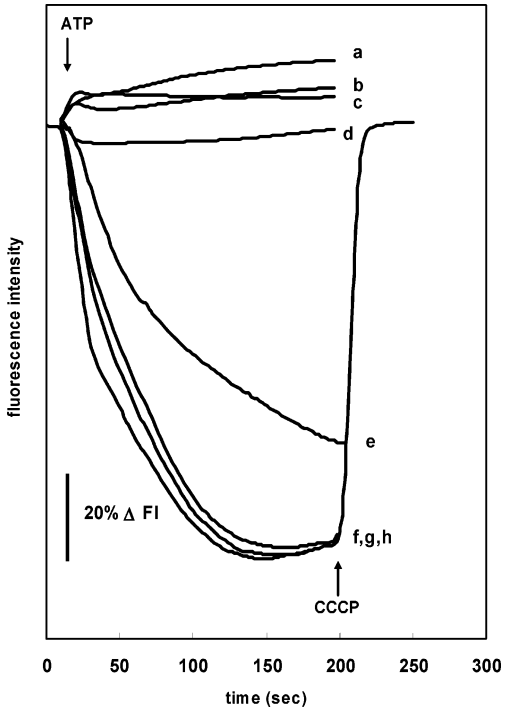

FIGURE 3: Formation of ATP-dependent electrochemical gradients measured by fluorescence quenching of 1 μM acridine orange in membrane vesicles from strains βD372V (a), γK9I/S12A (b), AN887 (c), γS12A (d), γK9I (e), γR7I (f), γS8A (g), and XL10 (h).

of the *E. coli* strain that contained the γR7I mutation was equivalent to the XL10 strain. This indicates that neither the putative salt bridge or hydrogen bond between γR7 or γS8 is important to ATP synthase activity.

Results of growth yields using 3 mM glucose as the sole carbon source followed the relative trend established in succinate-dependent growth assays (Table 2). Mutants γR7I, γS8A, and γK9I all had maximum optical density readings that were >90% of the XL10 value when grown on 3 mM glucose, while γS12A, γK9I/S12A, and βD372V attained only 66%, 56%, and 71%, respectively, of the XL10 value. The negative control *unc*-minus strain grew to 64% of XL10 on 3 mM glucose, providing further evidence that the poor growth exhibited by mutants γS12A, γK9I/S12A, and βD372V on minimal media with succinate was the result of impairment of the ability of F_1F_o to synthesize ATP.

Acridine Orange Fluorescence Quenching. Membrane vesicles obtained from mutant strains were analyzed for their ability to generate an electrochemical gradient via electron transport from the oxidation of succinate by the measurement of succinate-dependent fluorescence quenching of acridine orange (Figure 2). The extent of fluorescence quenching decreased to approximately 75−80% of the XL10 value with mutants βD372V, γS12A, and γK9I/S12A. In the γR7I and γS8A strains, the extent of fluorescence quenching was more than 90% of the XL10 value, while the γK9I strain achieved similar quenching to XL10.

The effects of the mutations on ATP-dependent proton pumping as measured by fluorescence quenching of acridine orange are shown in Figure 3. The strains carrying the γS12A, γK9I/S12A, and βD372V mutations were incapable of forming a proton gradient upon addition of ATP, while the γK9I mutant attained 72% of XL10 quenching capacity. The γR7I and γS8A strains attained essentially 100% of the quenching observed with XL10.

Kinetic and Thermodynamic Analysis of F_1-ATPase Activity. Figure 4 shows an Arrhenius plot of the Mg^{2+}-ATPase activity catalyzed by purified F_1-ATPase. With the exception of βD372V, the mutations did not significantly affect the temperature stability of the enzyme. A direct comparison of the effects of the mutations on k_{cat} was made at 25 °C as shown in Table 2 because the βD372V-F_1 was only stable to approximately 30 °C. The βD372V and γS12A mutations increased the rate of Mg^{2+}-ATPase activity by about 10−15% of XL10-F_1. However, the γK9I mutant decreased ATPase activity by about 2-fold. Consequently, the γR9−βD386 salt bridge in the $(ADP{\cdot}AlF_4^-)_2F_1$ structure appears to be important for EF_1-ATPase activity while the γS12−βD386 hydrogen bond observed in $(ADP{\cdot}AlF_4^-)_2F_1$ makes a small contribution to the rate-limiting step of ATP hydrolysis. The γR7I and γS8A mutants did not have a significant effect on ATPase activity. Since the γS12A and βD372V mutants resulted in large decreases in ATP synthase activity, the differential effects of the mutants on ATPase and ATP synthase activities were approximately 100-fold. Large differential effects on ATPase and ATP synthase activities were also observed with γK9I/S12A (nearly 70-fold).

The values for enthalpy, entropy, and free energy of activation for the ATP hydrolysis reaction were calculated from the data indicated by the lines in the Arrhenius plot at 25 °C as summarized in Table 4. The $\Delta G^{\ddagger}$ of XL10-F_1 at this temperature is 61.2 kJ mol^{-1}. Because k_{cat} is a function of $\Delta G^{\ddagger}$, any combination of $-T\Delta S^{\ddagger}$ and $\Delta H^{\ddagger}$ that sum to 61.2 kJ mol^{-1} will result in a k_{cat} equivalent to XL10-F_1. In the free energy plot of these data (Figure 5), isobars for k_{cat}

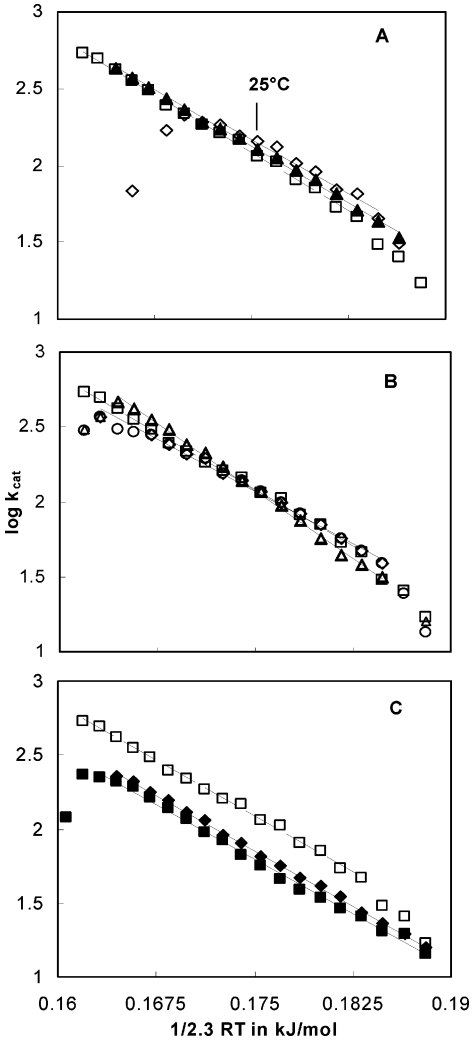

FIGURE 4: Arrhenius plot of Mg^{2+}-ATPase activity catalyzed by purified soluble F_1. (A) XL10-F_1, □; βD372V-F_1, ◇; and γS12A-F_1, ▲. (B) XL10-F_1, □; γR7I-F_1, △; and γS8A-F_1, ○. (C) XL10-F_1, □; γK9I-F_1, ■; and γK9I/γS12A-F_1, ◆. The concentration of F_1 was 3 nM for all analyses. Data points represent mean values from multiple analyses of each strain. Linear relations were generated by least squares regression of the data.

Table 4: Comparison of Thermodynamic Parameters for Steady-State MgATP Hydrolysis by F_1 Isolated from XL10 and from Mutants That Remove Interactions between the γ Subunit N-Terminus and βD372[a]

strain	E_a	$\Delta H^‡$	$T\Delta S^‡$	$\Delta G^‡$
XL10	50.2	47.8	−13.5	61.2
βD372V	49.2	46.7	−14.1	60.9
γS12A	48.3	45.8	−15.2	61.0
γK9I	51.7	49.2	−13.7	62.9
γS8A	46.1	43.6	−17.6	61.2
γR7I	62.1	59.6	−1.7	61.3
γK9I/γS12A	50.0	47.5	−15.0	62.5

[a] The parameters $\Delta H^‡$, $T\Delta S^‡$, and $\Delta G^‡$ were calculated at 25 °C from the data of Figure 4 as described in Experimental Procedures and are expressed in kJ/mol.

values at indicated percentages of XL10-F_1 activity are shown as diagonal lines. According to transition state theory, points in the lower left of this plot result when the rate-limiting step of the reaction contains more tightly bound reactants, and fewer bond rearrangements are required to complete the catalytic cycle. Points in the upper right result from more loosely bound reactants that require more bond rearrangements.

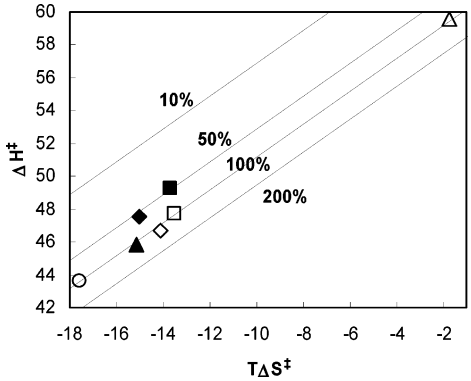

FIGURE 5: Free energy plot of Mg^{2+}-ATPase activity catalyzed by soluble F_1. Values for $\Delta H^‡$, $T\Delta S^‡$, and $\Delta G^‡$ were derived at 25 °C from Arrhenius data in Figure 2 for XL10-F_1, □; βD372V-F_1, ◇; γR7I-F_1, △; γS8A-F_1, ○; γK9I-F_1, ■; γS12A-F_1, ▲; and γK9I/γS12A-F_1, ◆. Isobars for $\Delta G^‡$ are shown as lines that are the percentages of XL10 k_{cat} values indicated.

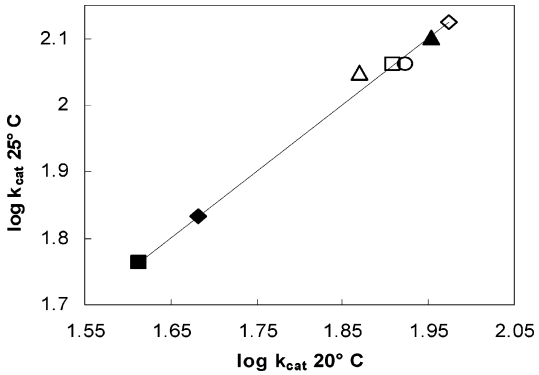

FIGURE 6: Linear relation in the isokinetic correlations of log k_{cat} at 20 °C vs log k_{cat} at 25 °C for ATPase activity catalyzed by XL10-F_1, □; βD372V-F_1, ◇; γR7I-F_1, △; γS8A-F_1, ○; γK9I-F_1, ■; γS12A-F_1, ▲; and γK9I/γS12A-F_1, ◆.

Mutants βD372V, γS12A, and γS8A decreased $\Delta H^‡$ with compensating changes in $T\Delta S^‡$ that left $\Delta G^‡$ (and thus, k_{cat}) about the same as XL10-F_1. Compensating changes in $\Delta H^‡$ and $T\Delta S^‡$ were also observed with the γR7I mutant, although the changes were in the opposite direction of the other mutants. The 2-fold decrease in k_{cat} observed with the γK9I mutant resulted from an increase in $\Delta H^‡$. The values of $\Delta H^‡$ and $T\Delta S^‡$ for the γK9I/S12A double mutant were intermediate to those of the individual mutants, suggesting that this was the sum of different effects caused by each mutant. It is noteworthy that this double mutant eliminates the possibility of forming both the γK9I−β_{DP}D372 salt bridge and γS12A−β_{DP}D372 hydrogen bond, as would the βD372V mutant. The values for $\Delta H^‡$ and $T\Delta S^‡$ of the latter mutant are also intermediate to those observed for the single γK9I and γS12A mutants.

In the isokinetic plot of the mutants shown in Figure 6, all of the mutants conformed to a straight line. Since a linear free energy relationship exists between the log k_{cat} at two temperatures for the rate-limiting step of any reaction, log plots that compare activities at two temperatures can determine if reactions have a similar rate-limiting step (*15*, *16*). The linear relationship observed among the mutants in Figure 6 suggests that the enzymes containing these

mutations all operate via the same rate-limiting step of the reaction.

DISCUSSION

In the $(ADP{\cdot}AlF_4^-)_2F_1$ structure from bovine mitochondria, βD386 ($EF_1\beta$D372) hydrogen bonds to γS12 ($EF_1\gamma$S12) and forms a salt bridge to γR9 ($EF_1\gamma$K9). Three mutations reported here that remove the ability to make one or both of these interactions between the β and γ subunits have similar effects on the function of the F_1F_o ATP synthase. Mutations βD372V and γS12A and double mutant γK9I/S12A decrease ATP synthase-dependent growth rate by nearly 2 orders of magnitude and eliminate the ability of the enzyme to catalyze ATPase-driven proton pumping. However, because the γK9I mutation does not significantly affect the ATP synthase-dependent growth rate and decreases ATP-dependent proton pumping by only 30% of that observed in the XL10 membranes, the results observed with double mutant γK9I/S12A primarily reflect the effects of γS12A. Consequently, in the course of catalysis the hydrogen bond and salt bridge do not appear to work as a single interlocking unit, and only the hydrogen bond observed between βD372 and γS12 is very important for the function of the F_1F_o holoenzyme.

Two possibilities to explain a complete loss of ATPase-driven proton pumping and a 2 order of magnitude decrease in ATP synthase-dependent growth rate, as reported here with mutants βD372V, γS12A, and γK9I/S12A, are (i) the loss of coupling between F_1 and F_o and/or (ii) incapacitation of ATP synthesis/hydrolysis at the catalytic sites. However, the membranes from these three mutant strains maintain 75−80% of the succinate-dependent proton gradient relative to that generated by XL10 membranes, and purified F_1 containing these mutations have substantial ATPase activity. A third possibilitiy is that the βD386−γS12 hydrogen bond formed in the $(ADP{\cdot}AlF_4^-)_2F_1$ structure is important for ATP synthase activity because it participates in the escapement mechanism hypothesis for F_1F_o-catalyzed ATP synthesis (*8*, *9*). In this mechanism, the transmembrane proton gradient provides constant torque to the γ subunit (via the c-subunit ring). However, the sum of hydrogen bonds and salt bridges between the γ and $\alpha\beta$ subunit ring prevents this rotation until the empty catalytic site binds substrate. After substrate-dependent disruption of several of these interactions between the γ and $\alpha\beta$ subunit ring, the torque on the γ subunit is greater than the energy in the remaining hydrogen bonds and salt bridges such that rotation of the γ subunit induces the conformational changes in the catalytic sites necessary for ATP synthesis.

If the $EF_1\beta$D372−γS12 hydrogen bond contributes to this escapement mechanism, this could explain the increased ATPase rates, the 20% uncoupling measured by succinate-dependent fluorescence quenching, and the extremely low ATP synthesis reported here due to the mutations that remove the ability to form this hydrogen bond. This $\beta-\gamma$ subunit interaction does not appear in the ground state structure (*6*) but only in the $(ADP{\cdot}AlF_4^-)_2F_1$ structure (*7*) in which the position of the γ subunit N-terminus is moved about 20° from the ground state position. During ATP hydrolysis, release of ADP and phosphate occurs to create an empty catalytic site with the final 40° counterclockwise rotation of the γ subunit (*5*). Consistent with this observation the data presented here suggest that, during ATP synthesis, enough clockwise rotation may occur to form the βD386−γS12 hydrogen bond even though one catalytic site remains empty. It is noteworthy that the c-subunit ring in EF_1F_o is believed to be a c10 oligomer (*17*) such that transport of a single proton across the membrane would rotate the γ subunit by about 36°. The rotation due to the slip of a single proton may allow enough flexibility to keep the 10 c-subunit ring aligned with the three catalytic sites during rotation.

The γK9I mutation decreases ATPase activity of purified F_1 by 2-fold, a decrease that is also observed in the γK9I/S12A double mutant, which suggests that the $MF_1\beta$D386−γR9 salt bridge observed in the $(ADP{\cdot}AlF_4^-)_2F_1$ structure is important for the ATP hydrolysis reaction. Due to the geometry of this salt bridge, and the direction of γ subunit rotation during ATP hydrolysis, the rotation will have the effect of compressing and strengthening the salt bridge while at the same time extending and weakening the hydrogen bond between $EF_1\beta$D372−γS12. The opposite will occur during ATP synthesis, which is consistent with the importance of the $EF_1\beta$D372−γS12 hydrogen bond in ATP synthesis. It is noteworthy that there is a 20° difference in the position of the γ subunit N-terminus between the $(ADP{\cdot}AlF_4^-)_2F_1$ and $(ADP)(AMPPNP)F_1$ structures from mitochondria (*6*, *7*), while the pause in rotation that results from the rate-limiting step of the ATPase reaction catalyzed by TF_1 occurs 40° prior to completion of one catalytic event (*5*). The effects reported here suggest that, in EF_1, the rate-limiting pause in rotation may occur at a point that more closely resembles the $(ADP{\cdot}AlF_4^-)_2F_1$ structure from mitochondria.

Although removal of the salt bridge by the γK9I mutation decreases k_{cat} by 2-fold, the βD372V ($MF_1\beta$D386) mutation does not exhibit a reduced k_{cat} (Table 2). In Figure 1, the backbone carbonyl of $MF_1\beta$D386 comes within about 5 Å of the $MF_1\gamma$R9 guanidinyl group and the γS12 hydroxyl such that the Coulombic attraction between these groups is significant. Because this carbonyl group is at the end of an α-helix, it will have the increased partial negative charge that results from the net dipole of the helix. Consequently, substitution of the βD372 carboxyl side chain with a hydrophobic group will not eliminate the attractive force of this residue for γK9. The removal of this carboxyl group will have a larger effect on the interaction with γS12 than with γK9, however, because the hydrogen bond between the backbone carbonyl and the γS12 hydroxyl is substantially weaker than that between the carbonyl and the guanidinyl moiety.

Figure 1 shows the sequential steps in a 120° γ subunit rotation during ATP hydrolysis assuming that the $(ADP{\cdot}AlF_4^-)_2F_1$ (*7*) and $(ADP)(AMPPNP)F_1$ (*6*) structures are good representatives of the intermediate and ground states of the catalytic cycle. In this model, the binding of Mg^{2+}-ATP to the empty catalytic site in Figure 1A induces the initial rotation of the γ subunit by 100° and thereby converts $(ADP)(AMPPNP)F_1$ to $(ADP{\cdot}AlF_4^-)_2F_1$ while at the same time results in the change in conformations of catalytic sites $\beta_E \rightarrow \beta_{TP}$ and $\beta_{TP} \rightarrow \beta_{DP}$ (Figure 1B) to initiate the rate-limiting step. During this step, the $\beta_{DP} \rightarrow \beta_E$ conformational change results in product dissociation that leads to the reversion of $(ADP{\cdot}AlF_4^-)_2F_1$ to $(ADP)(AMPPNP)F_1$ as

shown in Figure 1C. The tight winding of the coiled coil in $(ADP{\cdot}AlF_4^-)_2F_1$ is evident in the formation of the β_{DP}D386−γR9 salt bridge and the β_{DP}D386−γS12 hydrogen bond. The results presented here that show the importance of the β_{DP}-D386−γR9 salt bridge to ATPase activity suggest that energy stored in the tightly wound conformation of the coiled coil may contribute to the rate-limiting product release step.

It is noteworthy that although the γ subunit rotates 100° from Figure 1A to Figure 1B, the position of the γR9 side chain prior to rotation is only 4.8 Å from β_{TP}D386 with which it will form a salt bridge as the conformation changes to β_{DP}D386 (*6*). Although the MF_1 γR254 and γQ255 residues that engage the β subunit catch loop move counterclockwise 16−21 Å during this 100° rotation, the position of the γR9 side chain is such that it actually moves clockwise during this step as it makes a salt bridge to β_{DP}D386. Given the proximity of γR9 to β_{DP}D386 prior to rotation, it is possible that the affinity of these side chains for each other may help to initiate γ subunit rotation after ATP binds to the empty catalytic site. The results presented here support this hypothesis.

In a comparison of F_1 sequences from a wide variety of organisms (*14*), the γ subunit residue at position 9 is either an arginine or lysine, and thus the ability to form a salt bridge to $EF_1\beta$D372 is conserved. Both the βD372 and γS12 are also highly conserved in F_1 from a wide variety of species. A notable exception is that F_1 from the thermophilic bacterium PS3 contains γA12. This corresponds to the γS12A mutation reported here that resulted in a 2 order of magnitude decrease in the succinate-dependent growth of *E. coli*. It is possible that the sum of the energy in these hydrogen bonds between the $\alpha\beta$ ring and the γ subunit is more important to catalytic activity than their precise location. The presence of γA12 in F_1 from PS3 appears to be the result of an inversion in the sequence between a hydrophobic residue and the hydroxyl-containing side chain at positions 12 and 13 (Table 3) such that $TF_1\gamma$T13 may provide the hydrogen bond important to ATP synthase activity.

In the $(ADP)(AMPPNP)F_1$ structure, γR9 and γS12 have moved out of reach of β_{DP}D386 that instead forms a salt bridge with γR8 (*6*). In EF_1 this salt bridge would correspond to a hydrogen bond between β_{DP}D372 and γS8. The results presented here indicate that this putative hydrogen bond is not required for either ATP synthase or ATP hydrolysis activity. Although γS8 is not well conserved (*14*), in most cases the substitutions appear to be the result of an inversion between arginine and the hydroxyl group residues at positions 7 and 8 as is the case for *E. coli*. The results presented here indicate that the γR7I mutation does not influence catalytic activity significantly at 25 °C, although it does cause compensating changes in the enthalpy and entropy of activation, suggesting that this mutation requires an increase in bond rearrangements necessary to complete the reaction. Since the $\beta-\gamma$ subunit interactions that appear in the $(ADP{\cdot}AlF_4^-)_2F_1$ structure (*7*) and not in the ground state structure (*6*) are observed to affect the catalytic activity, this strongly suggests that the former structure is similar to the conformation of the protein during the rate-limiting step of the reaction.

ACKNOWLEDGMENT

We thank Kathy W. Boltz for insightful discussions and collaboration in method development.

REFERENCES

1. Senior, A. E., Nadanaciva, S., and Weber, J. (2002) The molecular mechanism of ATP synthesis by F_1F_o-ATP synthase, *Biochim. Biophys. Acta 1553*, 188−211.
2. O'Neal, C. C., and Boyer, P. D. (1984) Assessment of the rate of bound substrate interconversion and of ATP acceleration of product release during catalysis by mitochondrial adenosine triphosphatase, *J. Biol. Chem. 259*, 5761−5767.
3. Noji, H., Yasuda, R., Yoshida, M., and Kinosita, K., Jr. (1997) Direct observation of the rotation of F_1-ATPase, *Nature 386*, 299−302.
4. Yasuda, R., Noji, H., Yoshida, M., Kinosita, K., Jr., and Itoh, H. (2001) Resolution of distinct rotational substeps by submillisecond kinetic analysis of F_1-ATPase, *Nature 410*, 898−904.
5. Shimabukuro, K., Yasuda, R., Muneyuki, E., Hara, K. Y., Kinosita, K., Jr., and Yoshida, M. (2003) Catalysis and rotation of F_1 motor: cleavage of ATP at the catalytic site occurs in 1 ms before 40 degree substep rotation, *Proc. Natl. Acad. Sci. U.S.A. 100*, 14731−14736.
6. Abrahams, J. P., Leslie, A. G., Lutter, R., and Walker, J. E. (1994) Structure at 2.8 Å resolution of F_1-ATPase from bovine heart mitochondria, *Nature 370*, 621−628.
7. Menz, R. I., Walker, J. E., and Leslie, A. G. (2001) Structure of bovine mitochondrial F_1-ATPase with nucleotide bound to all three catalytic sites: implications for the mechanism of rotary catalysis, *Cell 106*, 331−341.
8. Greene, M. D., and Frasch, W. D. (2003) Interactions among gamma R268, gamma Q269, and the beta subunit catch loop of *Escherichia coli* F_1-ATPase are important for catalytic activity, *J. Biol. Chem. 278*, 51594−51598.
9. Chen, W., and Frasch, W. D. (2001) Interaction of the catch-loop tyrosine beta Y317 with the metal at catalytic site 3 of *Chlamydomonas* chloroplast F1-ATPase, *Biochemistry 40*, 7729−7735.
10. Senior, A. E., Latchney, L. R., Ferguson, A. M., and Wise, J. G. (1984) Purification of F_1-ATPase with impaired catalytic activity from partial revertants of *Escherichia coli* uncA mutant strains, *Arch. Biochem. Biophys. 228*, 49−53.
11. Kato, Y., Sasayama, T., Muneyuki, E., and Yoshida, M. (1995) Analysis of time-dependent change of *Escherichia coli* F_1-ATPase activity and its relationship with apparent negative cooperativity, *Biochim. Biophys. Acta 1231*, 275−281.
12. Shin, K., Nakamoto, R. K., Maeda, M., and Futai, M. (1992) F_oF_1-ATPase Gamma-Subunit Mutations Perturb the Coupling between Catalysis and Transport, *J. Biol. Chem. 267*, 20835−20839.
13. Gibson, F., Downie, J. A., Cox, G. B., and Radik, J. (1978) Mu-induced polarity in the unc operon of *Escherichia coli*, *J. Bacteriol. 134*, 728−736.
14. Hong, S., and Pedersen, P. L. (2003) ATP synthases: insights into their motor functions from sequence and structural analyses, *J. Bioenerg. Biomembr. 35*, 95−120.
15. Exner, O. (1973) The enthalpy−entropy relationship, *Prog. Phys. Org. Chem. 10*, 411−482.
16. Al-Shawi, M. K., Polar, M. K., Omote, H., and Figler, R. A. (2003) Transition state analysis of the coupling of drug transport to ATP hydrolysis by P-glycoprotein, *J. Biol. Chem. 278*, 52629−52640.
17. Fillingame, R. H., and Dmitriev, O. Y. (2002) Structural model of the transmembrane F_o rotary sector of H^+-transporting ATP synthase derived by solution NMR and intersubunit cross-linking in situ, *Biochim. Biophys. Acta 1565*, 232−245.

BI047293J